Nano-scale analysis of polymineralic surface coatings on aeolian quartz grains with palaeoenvironmental implications

Piotr KENIS[1, 2], Jacek SKURZYŃSKI[2, *] and Sandeep GORANTLA[1]

[1] Łukasiewicz Research Network - PORT Polish Center for Technology Development, Stabłowicka 147, 54-066 Wrocław, Poland; ORCID: 0000-0002-6152-3302 [P.K.], 0000-0002-8498-3651 [S.G.]

[2] University of Wrocław, Institute of Geography and Regional Development, Plac Uniwersytecki 1, 50-137 Wrocław, Poland; ORCID: 0000-0002-0965-7653 [J.S.]

The combined application of SEM/FIB cross-section lamella preparation and S/TEM characterization of individual aeolian quartz silt grains revealed two types of polymineralic coating (composed of Fe oxides/hydroxides, Al-silicates, together with relatively coarse incorporated crystals such as anhedral potassium feldspar and idiomorphic hematite) on the quartz grain, which differ in their internal structure (Type A – an openwork and relatively thick outer layer; Type B – a thinner and finer layer adherent to the grain surface). The highly porous Type B polymineralic coating may by disordered or arranged as laminae, and may lie directly on the quartz grain surface or may be separated by a thin layer of opal (with lepispheres) or cryptocrystalline quartz, most likely of diagenetic origin. These quartz grains, even in the silt fraction are not monomineralic monocrystals: monomineralic polycrystalline and even polymineralic polycrystalline internal structures with visible primary and secondary defects were found. All these characteristics of a coated quartz grain (including the opal/cryptocrystalline rims), in addition to the direct palaeoenvironmental interpretations, most likely can affect the accuracy and precision of age estimation using the optically stimulated luminescence (OSL) method; the rate of HF etching (hydrofluoric acid) is probably not uniform and isotropic as is assumed in OSL protocols.

Key words: FIB-S/TEM, electron diffraction, loess, polymineral coatings, dust individual particle analysis, OSL of loess deposits.

INTRODUCTION

Loess is a clastic deposit which consists predominantly of quartz particles 20–50 µm in diameter and which occurs as wind-laid sheets (Smalley and Vita-Finzi, 1968). There have been many reports on the physico-chemical and microphysical characterizations of such mineral dust because the environment in which it formed can be reconstructed on the basis of a variety of proxy data (e.g., Gallet et al., 1998; Rousseau et al., 2014; Kenis et al., 2020; Skurzyński et al., 2020; Baykal et al., 2021).

Loess researchers are exploring new research techniques, which allows them to overcome the previous limitations related to the small size of loess grains. This is particularly evident in mineralogical studies by scanning electron microscopy (SEM) integrated with energy-dispersive X-ray spectrometry (EDS) which, in case of automated mineral analysis, provides unattended, reproducible, and operator-independent elemental or mineral maps of relatively large mineral grain areas (Hrstka et al., 2018; Kenis et al., 2020).

SEM is also commonly used to describe the coatings or rims on such quartz grains (e.g., Weibel et al., 2010; Engelbrecht et al., 2016) or to interpret the microtextural features on the surface of individual quartz grains (e.g., Górska et al., 2023), but investigations of the internal structures of single dust particles are scarce (Jeong and Nousiainen, 2014). This is due to the limited possibilities to image directly the cross-section of a dust particle by conventional SEM and the need to use scanning/transmission electron microscopy (S/TEM) to study sub-surface layers a few nm thick. Especially rare are investigations combining the use of focused ion beam (FIB) thin-section (i.e. TEM lamella) preparation and high-resolution transmission electron microscopy (Jeong and Nousiainen, 2014) despite the promise of this approach. For example, a recent FIB-TEM analysis (Górska et al., 2023) revealed that the development of surficial marks on a quartz grain can be profoundly influenced by both primary (e.g., inclusions, grain boundaries) and secondary (e.g. frost-induced cracks) crystal defects. Until now, this kind of data (FIB-TEM) for a dataset of aeolian grains has only been available for dust particles in Asia (Jeong and Nousiainen, 2014); the most thorough research on dust so far has been done for optical modeling in the context of interactions of mineral dust with incoming/outgoing electromagnetic radiation in the atmosphere (Moosmüller et al., 2012; Jeong and Nousiainen, 2014; Engelbrecht et al., 2016).

The optical properties of quartz grains are used for assessing the age of a geological deposit, including in numerical dating by luminescence methods in the geosciences and archaeology (Moska et al., 2021). Establishing the luminescence age requires specific procedures for sampling, material preparation, and different types of measurements (e.g., Moska, 2019). For the purposes of this article (omitting for now the previous steps of material preparation such as grain size selection, removing of carbonates and organic matter, density separation etc.) we focus on the final step, etching with concentrated (40%) hydrofluoric acid (HF) for 1 h, to remove the outer layer of the (~10 µm) quartz grains that absorb the alpha radiation dose (Aitken, 1985, 1998) – i.e. particles with an energy of 1 MeV will have a 3.3 µm projected range in quartz (Berger et al., 1999). A simplified manner of expression is frequently used, such that non-quartz components (such as polymineralic/clay coating or minerals that might be still present after density separation) are dissolved (Bell and Zimmerman, 1978), quartz grains are etched isotropically, and the rate of quartz etching is known (Porat et al., 2015; Duval et al., 2018; Poręba et al., 2022). This assumption is directly related to the accuracy and precision of the estimated age (Poręba et al., 2022); however, quartz etching is an anisotropic phenomenon, and the assumption of grain sphericity may commonly be an oversimplification (Poręba et al., 2022 and the references therein).

In addition, a 'single' particle is rarely a single crystal or mineral, but commonly it is a polycrystalline or polymineralic form (Falkovich et al., 2001; Jeong, 2008; Jeong et al., 2014); an example may be mosaic internal structure of quartz (Frederickson 1955; Górska et al., 2023). Intergrowths and the composite mineral clusters are also common (Engelbrecht et al., 2016), and so the microphysical data obtained from a 'single' particle are often the result of the interaction of numerous mineral grains, composed of different mineral types (Jeong and Nousiainen, 2014).

The assumption of a single grain of quartz can be further complicated by the presence of various kinds of non-quartz coatings or rims covering its surface (Jeong and Nousiainen, 2014; Engelbrecht et al., 2016), potentially related to different palaeoenvironmental conditions – e.g. soil-forming processes (Biernacka and Issmer, 1996), especially in the immediate vicinity of aquatic environments, have often been emphasized (e.g., Lee et al., 2013; Wooldridge et al., 2019 and references therein). Of course, aluminosilicate coatings are usually removed (or the authors assume they have removed them; Bell and Zimmerman, 1978) before microtextural analysis (e.g., Górska et al., 2023) or Optically Stimulated Luminescence (OSL) dating (e.g., Moska et al., 2021) but little is known about their internal structure.

In this study, we explored both individual dust grains and the internal structures of their coating types by high-resolution TEM (HR-TEM). Electron-transparent thin lamellae were prepared for TEM analysis using typical SEM/FIB-based TEM cross-section sample preparation (Schaffer et al., 2012). The crystal structural details of grains from representative Polish loess deposits are described, with discussion of the implications for generally accepted paleoenvironmental interpretations. Our results may also contribute to geotechnical concerns, with particular emphasis on the process of collapse in loess.

MATERIALS AND METHODS

The combined application of site-specific FIB cross-section lamella preparation and S/TEM characterization is a powerful method for imaging the internal structures of dust grains (Jeong and Nousiainen, 2014). Unfortunately, FIB cutting cannot be applied to many grains because it is expensive and requires complex operation (Jeong and Nousiainen, 2014), so three coated particles were randomly selected (after prior macroscopic analysis of an ion-thinned bulk sample; see Section 2.1) from the loess samples stored in the Department of Physical Geography of the University of Wrocław. Previously, thousands of grains had been classified into minerals and mineral groups based on their morphological and chemical characterization by extensive Scanning Electron Microscopy (SEM) and Energy-dispersive X-ray Spectroscopy (EDS) investigations (Skurzyński et al., 2020; Kenis et al., 2020 and unpublished data). The analyses were made in the Łukasiewicz Research Network – PORT Polish Center for Technology Development in Wrocław, Poland.

The quartz grains selected represent three well-recognized Polish loess-palaeosol sequences, those of Biały Kościół (Moska et al., 2019), Złota (Moska et al., 2018; Skurzyński et al., 2020) and Tyszowce (Moska et al., 2017; Skurzyński et al., 2019), developed in the domain of the northern European loess belt (domain II sensu Lehmkuhl et al., 2021) but potentially under the different palaeoenvironmental conditions (e.g., Maruszczak, 1991): Biały Kościół belongs to subdomain IIb (Western European continental subdomain), and the other sections to subdomain IIc (Central European continental subdomain; Lehmkuhl et al., 2021). The samples from Biały Kościół (2.6 m b.g.l.) and Tyszowce (9.10 m b.g.l.) are correlated with MIS2 (L1LL1; Marković et al., 2008, 2015), and the sample from Złota (9.85 m b.g.l.) with MIS4 (L1LL2; Marković et al., 2008, 2015). This allows the preliminary recognition of the loess as from both main loess units of the last interglacial-glacial cycle in Poland.

The analysis of three coated quartz grains may not be sufficient to illustrate the overall variability of the coating types on loess particles in Poland; nevertheless, Jeong and Nousiainen (2014) stated that FIB-TEM investigation of 35 particles of differentiated mineral phases was representative of dust in Asia. In this work, we describe our preliminary research results to demonstrate the potential of such qualitative analysis to aid interpretation, and to emphasize the scientific impact it may have in the geosciences with further refinement of the methodology. The number of grains investigated will be increased as this research develops.

TIC 3X ION PREPARATION

The first step to assess the frequency (or relative amount) of coated quartz grains was ion polishing (by Ar ions using a *Leica TIC 3X* ion polisher) of a bulk sample of thousands of loess grains. In this way (Fig. 1B) a cross-section of the sample was obtained (Fig. 1A), avoiding any mechanical damage or disturbance. This revealed that relatively thick coatings are widespread, allowing flexibility in selecting particles for higher resolution tests using TEM/STEM. This means, that by analyzing a standard SEM image (without ion-thinning), it is possible to initially identify whether a particle is coated (Fig. 1C) or not (Fig. 1D).

FIB LAMELLA AND TEM IMAGING

TEM cross-section specimens (i.e. FIB lamellae) of coated quartz grains were prepared using a conventional in situ lift-out FIB procedure in dual beam SEM. In brief, the samples were initially coated with a 40 nm-thick amorphous carbon layer using a *Leica EM ACE600* sputter coater. A Thermo Fisher Scientific
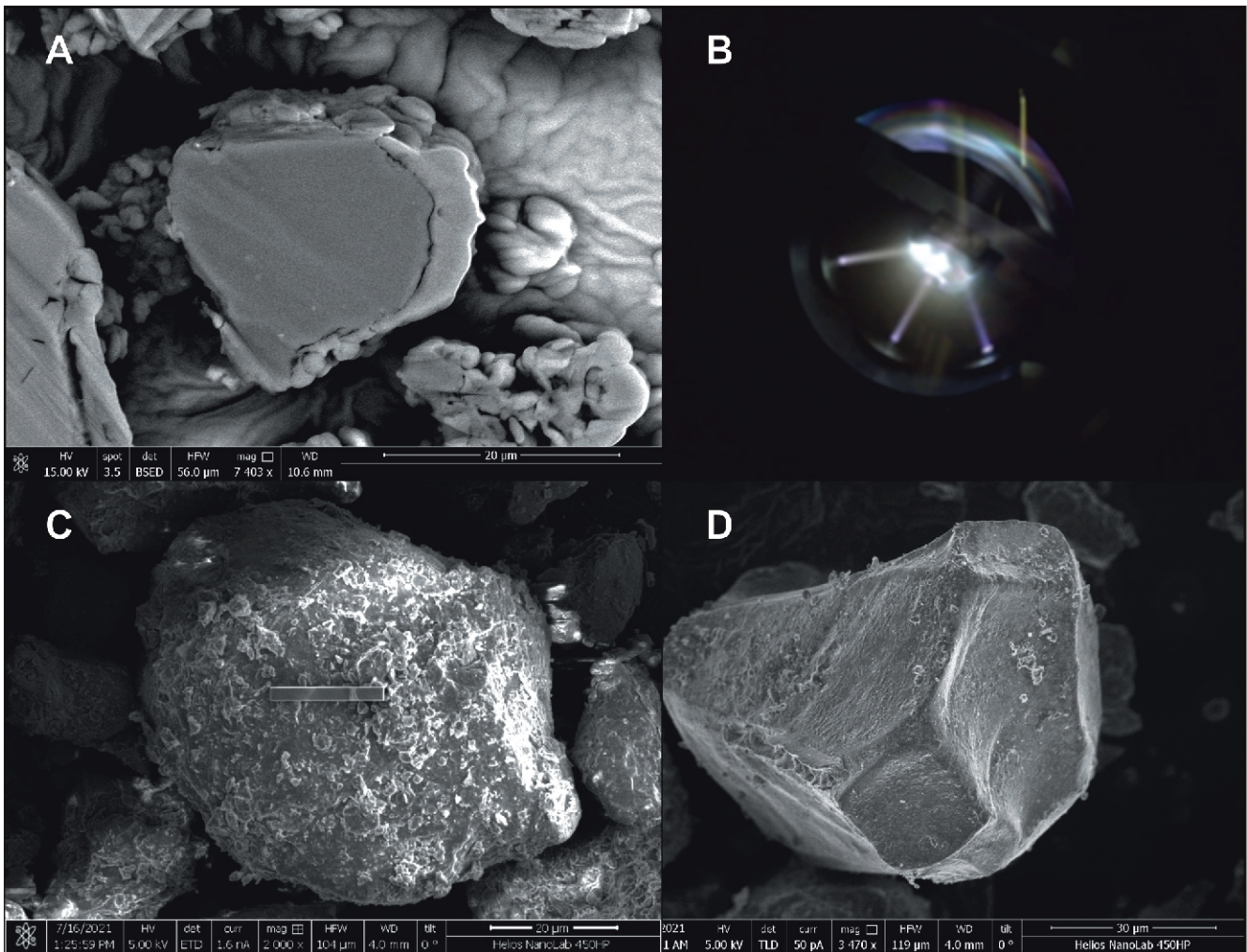
Fig. 1A – an example of a grain cross-section from the ion-thinned bulk sample; B – ion-thinning in progress; C – a coated mineral grain before ion-thinning; D – a non-coated mineral grain

Helios Nanolab 450HP SEM/FIB equipped with a Ga-ion beam source was used for FIB lamella preparation. Both electron- and ion beam-assisted Pt layers were deposited to prevent any surface damage to the sample. After lifting out and welding the lamellae to TEM half grids, thinning of the lamellae was performed in successive steps by gradually lowering the ion beam currents from 2.5 nA to 80 pA at 30 kV until a thickness of 150 nm was reached in the electron-transparent section of a lamella. Further thinning and final polishing was done by steps of 5 kV, 41 pA; 2kV, 23 pA and 1kV, 29 pA. The sequential course of the entire process of preparing lamellae is shown in Figure 2.

HAADF-STEM investigations were performed on a *Thermo Fisher Scientific Titan 60-300* cubed TEM equipped with an X-FEG electron source, dual Cs-correctors, and a Super-X X-ray energy dispersive spectrometer (EDS). The imaging was performed in a STEM high angle annular dark field (STEM-HAADF) mode detector. The HAADF-STEM imaging parameters used in this study were accelerating voltage of 300 keV, electron beam probe current of 100 pA, beam semi-convergence angle of 21.4 mrad and detector collection angles in the range of 50.5–200 mrad. STEM image (1024 x1024 pixels) acquisition was done using 18 µs pixel dwell time. X-ray EDS elemental mapping was performed in spectral imaging mode.

The minerals described in this paper were identified on the basis of elemental composition by the EDS method, and, especially for illite-smectite clay minerals (ISCMs) by the measurement of d spacing in relation to published data (Arnold, 1962; Levien et al., 1980; Downs et at., 1993; Hirose et al., 2005; Ikuta et al., 2007; Jeong and Nousiainen, 2014; Fig. 3). An example of way of ISCM identification based on the spacing of repeat units measured from a TEM lattice fringe image is shown in Figure 3H–J, including the problems of partial amorphization during the imaging (Fig. 3G; traces of Ga-ions are also visible). The means of reliably distinguishing between quartz and opal is also shown (Fig. 3A–F).

RESULTS AND DISCUSSIONS

Coatings on glacigenic sediment grains in Poland have not been widely studied even using SEM (TEM research is scarce globally). The most extensive research on this topic was carried out in order to explain the process of collapse in loess (Grabowska-Olszewska, 1983), where a general theoretical model of coating structure was proposed: on a primary "core" grain made of quartz (a ditrigonal pyramid with dimensions of the order of 10–50 µm, made of many crystals separated by lin-
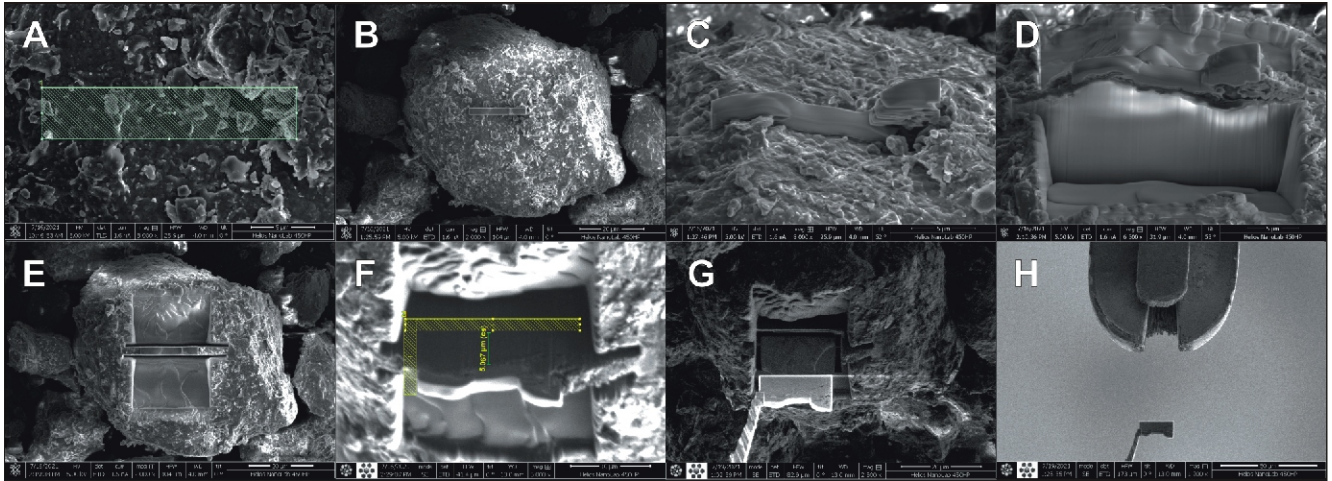
Fig. 2. Montage of sequential SEM/FIB cross-section TEM lamella preparation steps from a coated quartz grain, from the Złota profile

A – the rectangle shows the area of an individual grain from which the lamella is be obtained. It also indicates the region where e-beam and ion-beam Pt protection is deposited as the first step; **B** – shows an overview image of this whole quartz grain after the Pt-protection layer deposition step; **C** – shows the cross-section view of the sample area after this step; **D** – tilted view of one face of the lamella after removing the material; **E** – top view showing milled trenches on both sides of the lamella; **F** – markers showing the region of final cutting of the lamella from the bulk samplep; **G** – lamella extraction with tungsten needle; **H** – showing the approach of the needle with lamella towards the TEM grid, the final transfer step

ear defects) there is a thin coating of amorphous SiO_2 gel, and on this a highly porous coating of finely dispersed calcium carbonate ($CaCO_3$). On this, in turn, there is a polymineral coating, made of clay minerals (forming microaggregates), iron oxides and hydroxides, amorphous silica, dispersed carbonates and finely dispersed quartz. The general veracity of the model (Grabowska-Olszewska, 1983) developed on the basis of regular SEM observations, is justifiable; however, it requires refinement using more advanced and accurate analytical methods.

In order to test the model established by Grabowska-Olszewska (1983), the starting point was the initial ion polishing (see: Section 2.1) coupled with SEM imaging, which showed that the 'polymineral coating' (Grabowska-Olszewska, 1983) or 'surface coating' (e.g., Engelbrecht et al., 2016) visible in the SEM microscope is heterogeneous. It can be divided into: (1) a relatively coarse (~10 micron scale) part of openwork character, made mainly of randomly arranged minerals with a lamellar shape (Type A in Fig. 4), and (2) a finer part, adhering relatively closely to the grain, usually filling cavities and gaps on the grain surface (Type B in Fig. 4). The first of these, with a structure easily observable by SEM, is commonly reported and will not be described in detail in this paper. The second one will be discussed more extensively as well as the near-surface parts of the quartz grain (i.e. the quartz/coating transition).

ZŁOTA LOESS SEQUENCE

Examination of the strongly adhesive part of the coating (Type B in Fig. 4) on the surface of the FIB lamella from Złota (Fig. 2) revealed a complicated internal structure (imperceptible in SEM). It is clearly visible, both on TEM images and EDS elemental maps (Fig. 5) mainly due to the alternating arrangement of phases containing Fe oxides/hydroxides (Fe in Fig. 5B) and Al-silicates (Si in Fig. 5B – as seen in Fig. 5D, the layers enriched in Si and Al overlap so, for ease of perception, is limited to Si in Fig. 5B). The mutual relationship between the layers enriched in Fe and those dominated by Si (a kind of discrete multilayer structure) is particularly clearly visible in the thicker part of the Type B polymineralic coating (Fig. 5B), however, Al

and Mg also clearly indicate the linearity of the overall structure (Fig. 5D). The above-described linear internal structure is characteristic also of the thinner part of the Type B polymineralic coating (Fig. 5C). This linearity is clearly visible even in a mineral substrate partially degraded/amorphized due to the TEM imaging (e.g., Lee et al., 2007) – e.g. in the amorphous part of the polymineralic Type B coating, clay platelets composed of ISCMs can be found (Fig. 3G, I and J).

The laminated coating described looks like a flow-related structure (Fig. 5B), and the thicker part of the Type B coating shows various types of plastic deformation of the layers (i.e. folds, boudins, discontinuities, etc.), while extraneous inclusions (in this case potentially bacteria; Blanco et al., 2010) within these layers were also detected (Fig. 6B).

Interestingly, TEM analysis of the grain from Złota showed, in accordance with the model of Grabowska-Olszewska (1983), the presence of amorphous silica (opal) on the surface of the quartz grain. The boundary between the quartz 'core' and the hydrated silica is very sharp and clearly visible (Fig. 5A). The opal tightly covers the quartz surface with interconnected spherical forms (Fig. 5A) of various sizes (from 1 µm to several tens of nm) called lepispheres (Flörke et al., 1976; Weibel et al., 2010). Smaller opal lepispheres are clearly visible (Fig. 6C) and resemble the early diagenetic opal described by Weibel et al. (2010) in marine sediments. The wave-shaped structures (Fig. 5A) known from precious opals are also visible in the internal structure of the opal in the grain examined, which may indicate the flow of the silica colloid (Liesegang and Milke, 2018).

The relations between the Type B coating and the opal substrate are not always sharp and obvious, as in the case of the quartz/opal boundary. In some places unfilled pore spaces (Fig. 5B) can be found. In other areas the opal-made structures are mutually interspersed with each other (Fig. 6D) or even with non-opal structures (Fig. 6B), probably the result of complicated geometry and intersection, and not alternating growth.

As the uppermost part of the coating, an outer carbonate rim (probably of post-depositional genesis) with clearly visible layering was observed in several places. If present, it adheres directly to the aluminosilicate-iron part of the coating (Fig. 6A).
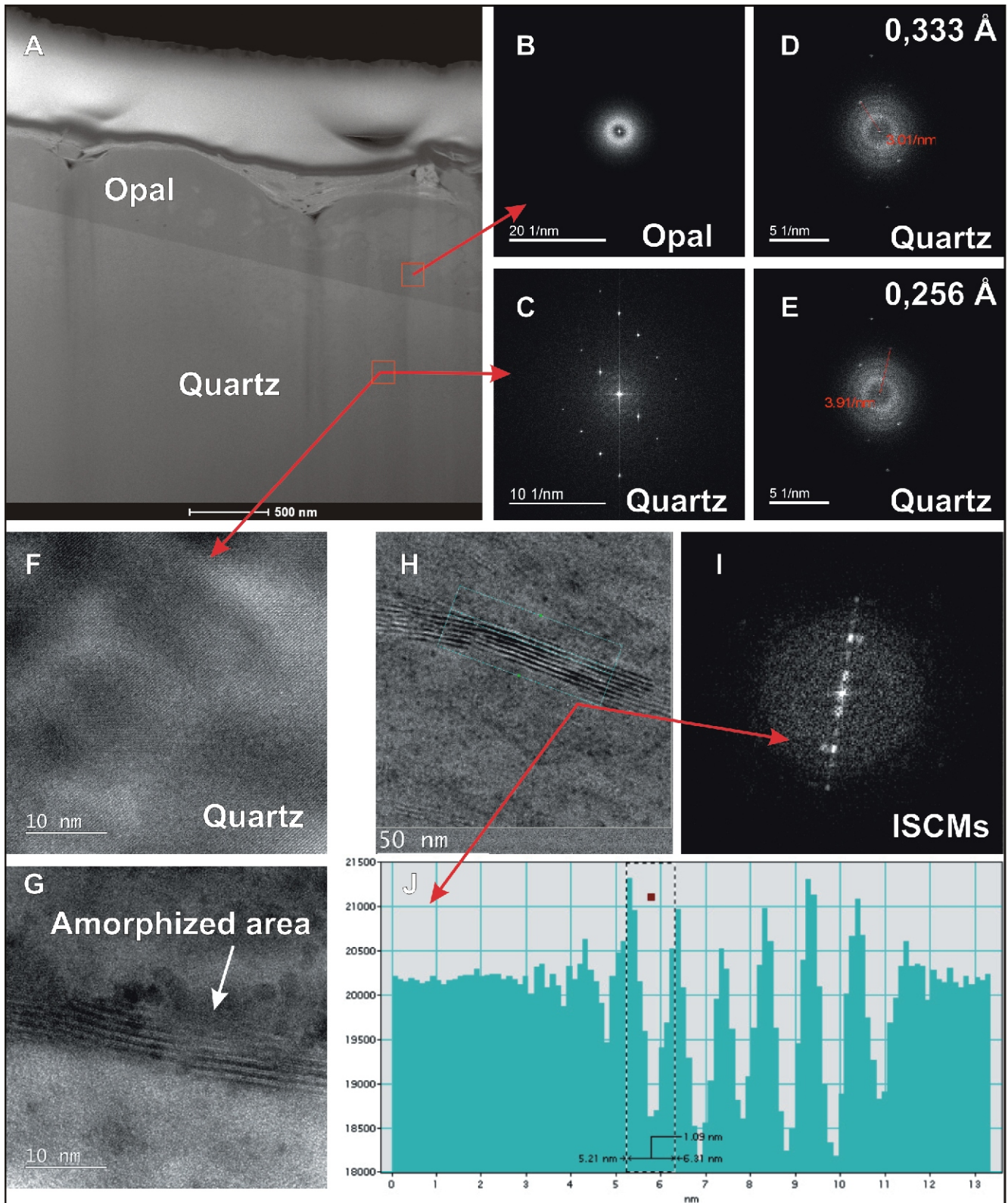
Fig. 3. The means of ISCMs identification, and distinguishing opal from quartz

A – HAADF-STEM cross-section overview image showing clearly the ISCMs, opal and quartz layers; **B** – the FFT pattern of a HRTEM image from the opal region shown clearly indicates that this phase is amorphous; **C**–**E** – shows the FFT patterns from different regions in the HRTEM image; **F** – this clearly indicates that the quartz is monocrystalline; **H** – shows the HRTEM image with lattice fringes from the ISCMs layer; **J** – corresponding FFT pattern from marked rectangle region in (H), and image intensity profile across the lattice fringes in (J) with interlayer spacing ~ 1.1 nm
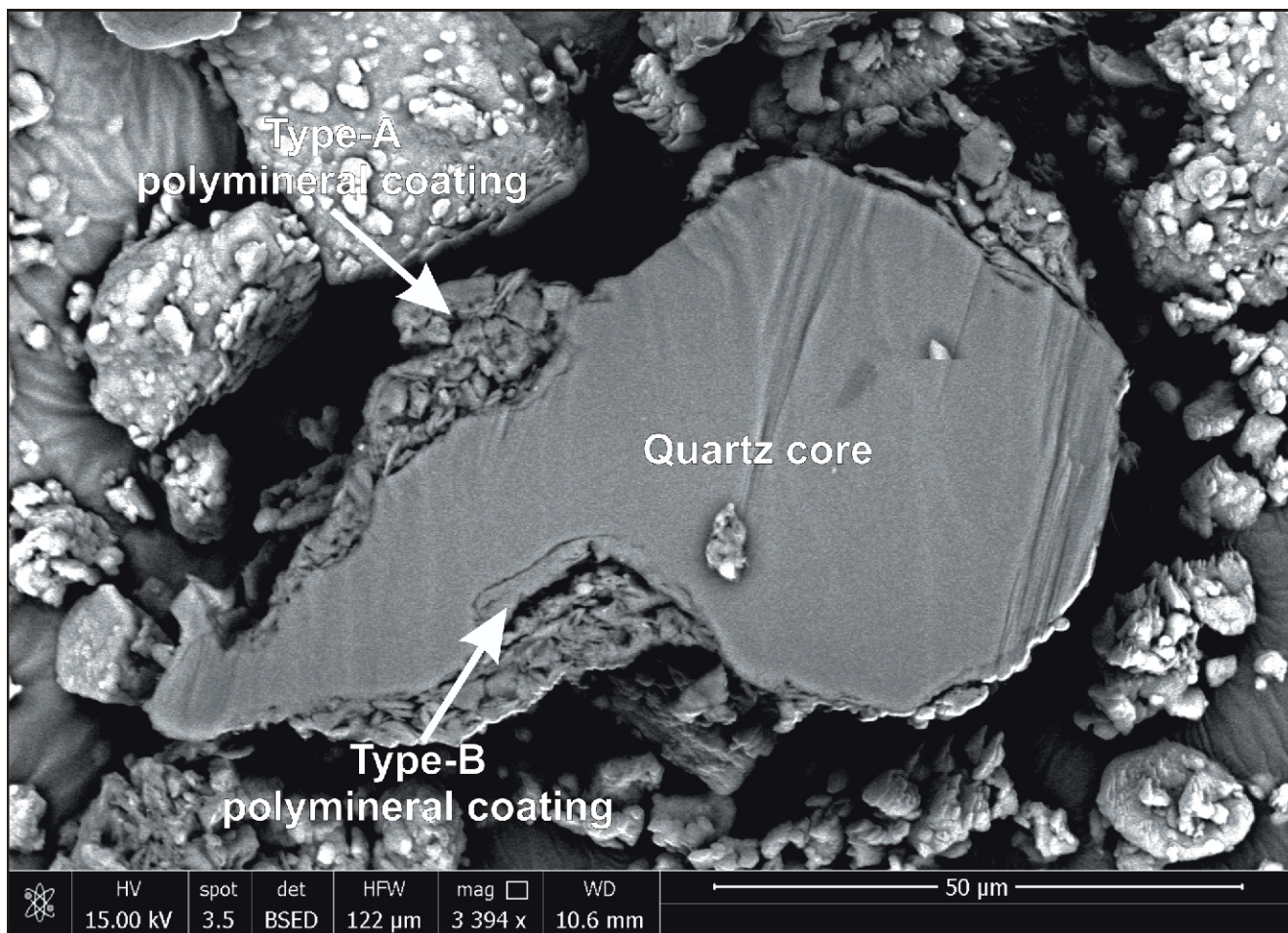
Fig. 4. The ion-thinned cross-section of the quartz grain from Złota showing variability of the polymineralic coating (Type-A and Type-B are described in the the text)

BIAŁY KOŚCIÓŁ LOESS SEQUENCE

The coating observed on the loess grain from Biały Kościół section is generally composed of lamellar minerals and iron-rich phases (Fig. 7). However, relatively large objects up to 300 nm across, such as sharply edged anhedral potassium feldspar and an idiomorphic hematite crystal below, were also found (Fig. 7A). The most important feature of the polymineralic coating from the Biały Kościół, distinguishing it from the grain from Złota, is its disordered structure, clearly visible on the EDS map for Al + Fe (Fig. 7D), as well as in the irregular arrangement of other elements (Fig. 7D). However, despite the relatively random arrangement and lack of continuity of the layers, the minerals are arranged parallel to the surface of the quartz grain examined. The lamellar minerals generate a large number of pore spaces within the coating (Fig. 7A), and in contact with the quartz (Fig. 7B). The pore spaces are also present between larger mineral phases and the ISCMs (Fig. 7A). The pore space formed at the interface between a potassium feldspar and lamellar minerals mirrors the shape of the edge of the larger particle. These features give the Type B coating from Biały Kościół an open structure, although much finer than of the Type A coating (Fig. 4).

Unlike the grain from Złota, and not in accordance with the Grabowska-Olszewska (1983) model, no opal rim was found on the grain from Biały Kościół. However, there is a clearly visible polycrystalline, 'mosaic' (Frederickson, 1955), internal structure of the quartz (Fig. 8).

TYSZOWCE LOESS SEQUENCE

The polymineralic coating on the tested particle from Tyszowce is generally composed of clay minerals and phases rich in Fe. Alternating layers are visible (Figs. 10 and 11), which were also well developed in the Złota sample (Fig. 5), but not found in the Biały Kościół (Fig. 7) sample. The Type B coating from Tyszowce is characterized by high porosity (Figs. 10 and 11), and it is thickest (Fig. 10) above the depressions in the quartz surface, similarly to the situation in the Złota (Fig. 5) sample.

The Tyszowce grain showed a heterogeneous internal structure of quartz (Fig. 12), as with the Biały Kościół grain (Fig. 8), it is not a monomineralic crystal. Firstly, the quartz which is the central part of this grain has an outer rim of ~300 nm of the cryptocrystalline variety of this mineral (Fig. 11). This layer of cryptocrystalline quartz is thinner than the amor-
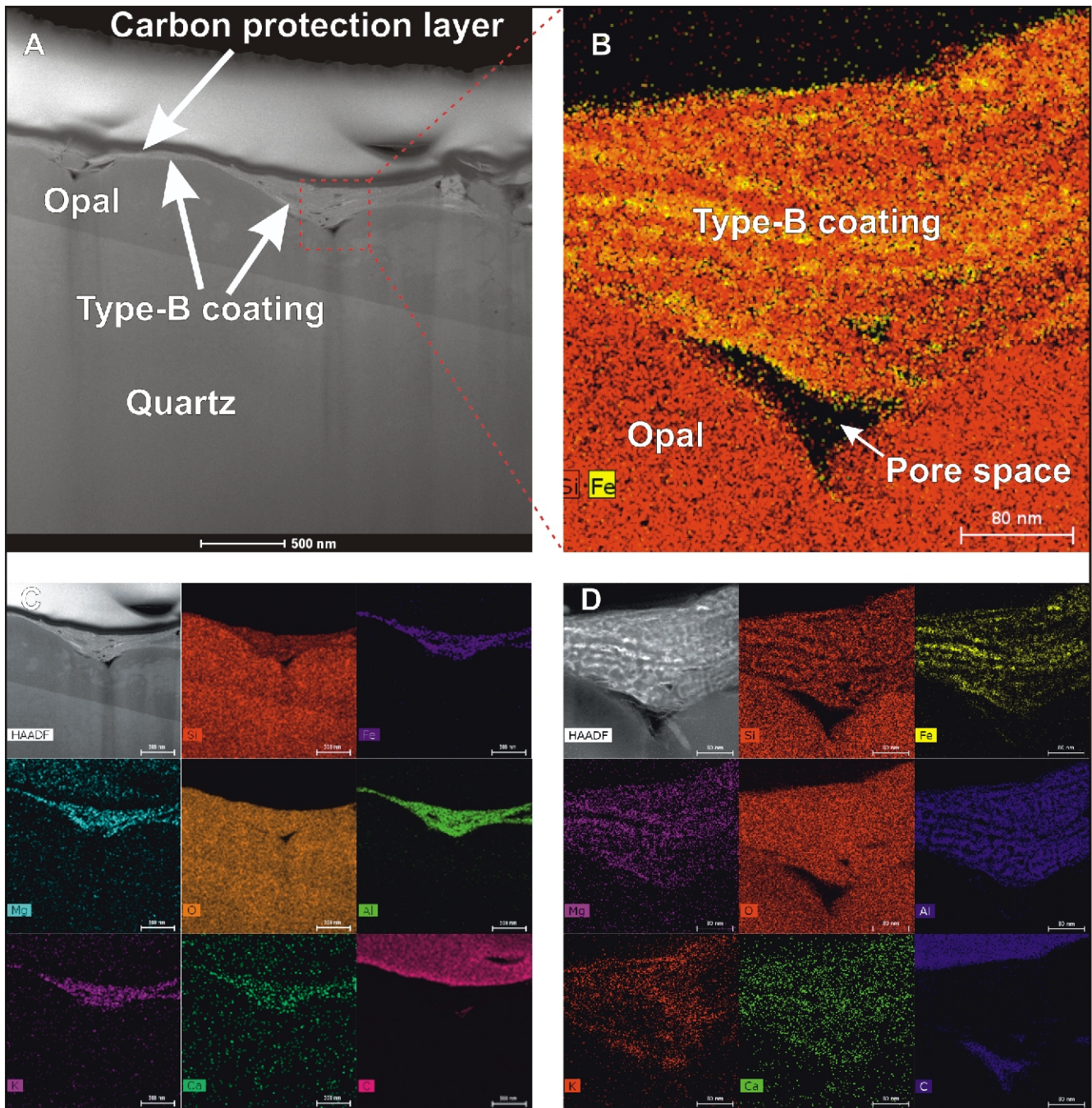
Fig. 5A – overview HAADF-STEM image of the Złota grain cross-section with different layers of coating, Type B polymineralic layer of varying thickness, and the opal rim layer on the quartz surface; B – elemental EDS map showing Si and Fe distribution in a thicker region of the Type B polymineralic coating; C, D – an EDS elemental maps montage of the overview and magnified region of the thicker polymineralic layer respectively

phous opal in the Złota sample, but its structural location and relations to the other individual components of the grain are similar (Fig. 5). Within the quartz 'core', mica inclusions (Figs. 10 and 12) and structural deformations are visible (Fig. 12). Two generations of crystalline quartz were observed (quartz core and quartz overgrowth; Haile et al., 2021), separated by a thin layer of cryptocrystalline quartz (Fig. 12).

THE IMPLICATIONS OF COATING INTERNAL STRUCTURES
AND NEAR-SURFACE PARTS OF THE QUARTZ "CORE" FOR
PALEOENVIRONMENTAL INTERPRETATIONS

The preliminary analysis of the aeolian quartz grains analysed (representing loess sections from different regions of Poland), based on the initial ion polishing coupled with SEM imag-

ing, showed that the parts of the polymineralic surface coatings are heterogeneous. They can be divided into: (1) a relatively coarse (up to about ten microns) part of openwork character, composed mainly of randomly arranged minerals with lamellar shapes (Type A in Fig. 4), and (2) a finer part, adhering relatively close to the individual quartz grain surfaces, often filling cavities and gaps along the quartz grain surfaces (Type B in the Fig. 4).

Detailed examination of the Type B polymineralic coatings by S/TEM revealed differences in internal structure between the ordered (Złota and Tyszowce; Figs. 5 and 11, respectively) and disordered (Biały Kościół; Fig. 7D) settings. It was also seen that a Type B polymineralic coating may be attached to the quartz surface (such as at Biały Kościół; Fig. 8). However, amorphous silica (Złota; Fig. 5) or cryptocrystalline quartz
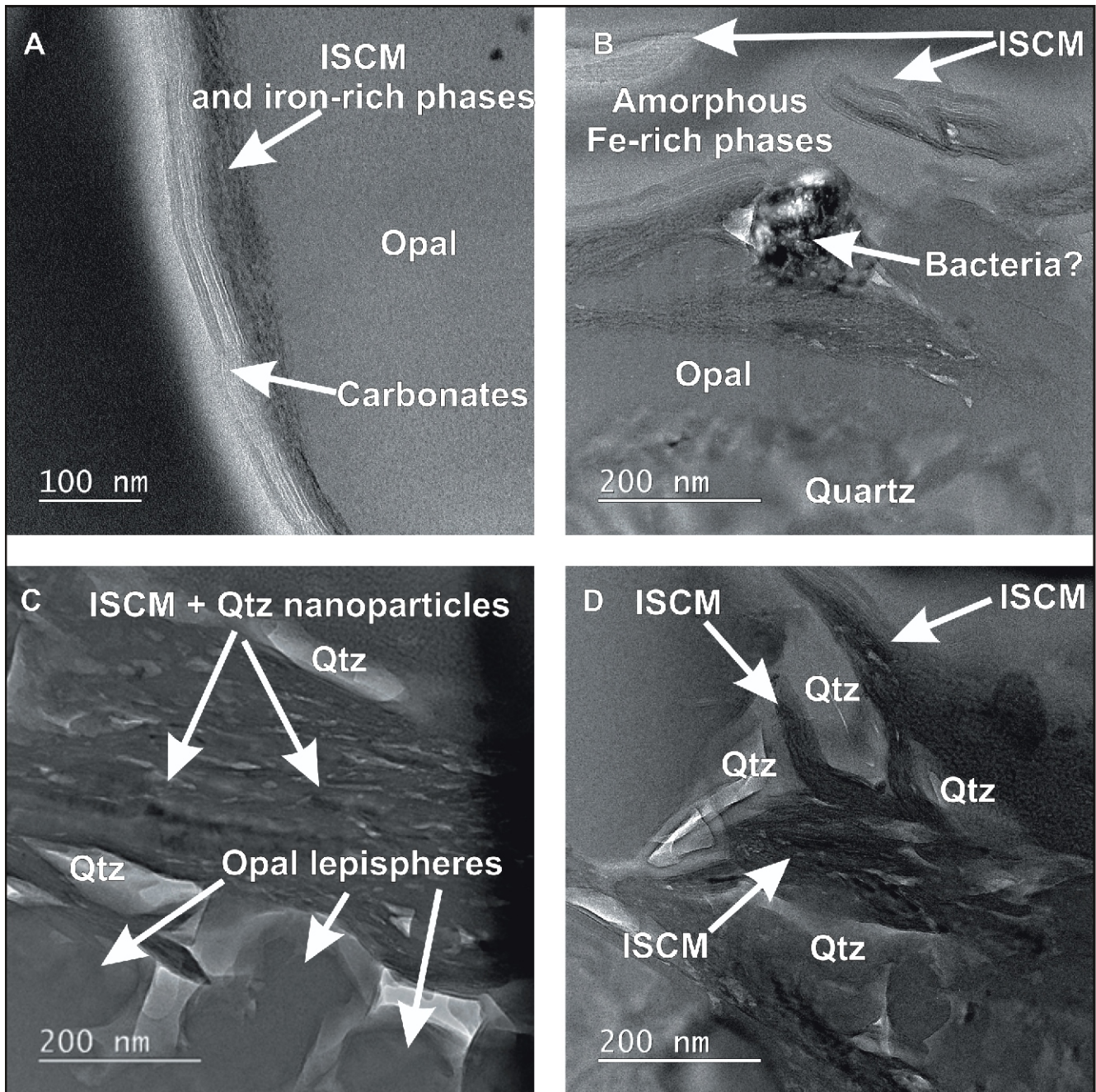
Fig. 6. TEM images showing differences in the structure of the coating in different areas of the grain

A – thin polymineralic coating, underlying a carbonate coating with clearly marked layering; **B** – discontinuities and structural disturbances in the coating on the boundary with the foreign carbonate particle (probably a bacterial microfossil); **C** – ISCM overgrowths with opal lepispheres and microcrystalline quartz; **D** – ISCMs tightly surrounding microcrystalline quartz sub-grains

(Tyszowce; Fig. 12) may also be found at the transition between the polymineralic coating and the quartz surface. In each of the grains examined, elements of the particle coatings noted by Grabowska-Olszewska (1983) were found. However, the conceptual model was not fully reflected in the measurements. In addition, the Grabowska-Olszewska (1983) model is insufficient for more precise interpretation of the constituent elements of the opal and cryptocrystalline quartz rims on the grains studied. For this reason schematic trends of quartz authigenesis through early and late diagenesis (Weibel et al., 2010) have been studied (Fig. 12). Two of the grains investigated (Złota

and Tyszowce) bear clear traces of both early and late diagenesis (Fig. 12). In one of the grains (Tyszowce) variability in the intensity of diagenetic processes was documented (Fig. 12C, D). The grain shows signs of early diagenesis (inner cryptocrystalline quartz rim, Fig. 12C), followed by late diagenesis (macroquartz or quartz outgrowth. The extent of the original grain remains unknown; Fig. 12C), and of early diagenesis (outer cryptocrystalline quartz; Fig. 12D). These features of the grains studied can be matched to the C1 trend of quartz authigenesis through early and late diagenesis (Weibel et al., 2010): *Lepispheres – circular cavities (due to dissolution*
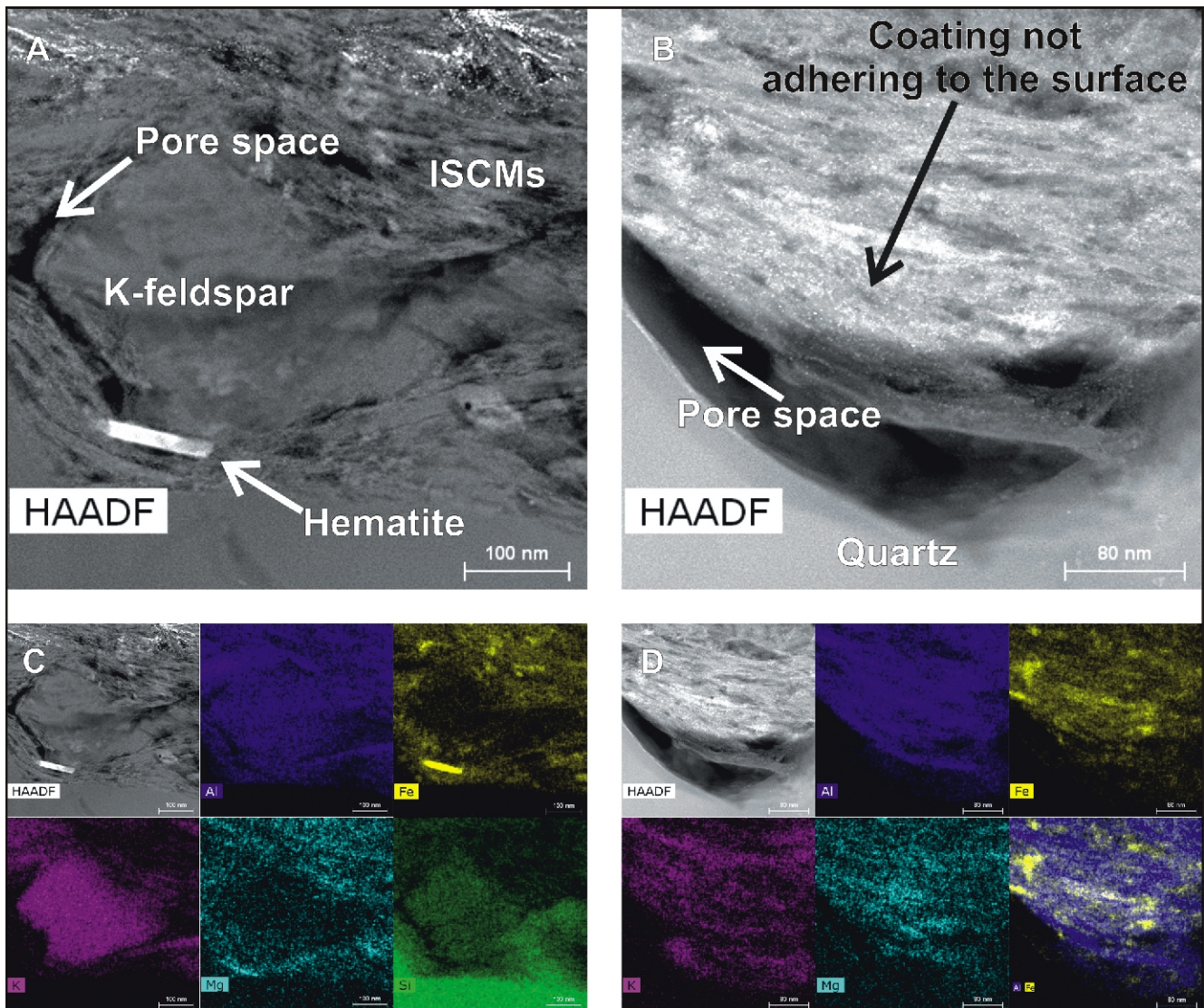
Fig.7A and C – HAADF-STEM and EDS mapping images of an irregular coating structure with a K-feldspar and a hematite crystal below, surrounded by ISCMs.; B and D – HAADF-STEM and EDS mapping images of a Type B coating not adhering to the surface of the quartz in a U-shaped recess

of lepispheres) in ordered microquartz coating – random microquartz as the thickness of the coating increases - quartz outgrowths in circular cavities – merging of outgrowths into macroquartz; and the outer cryptocrystalline quartz rim (Fig. 12D) in the particle from Tyszowce resembles the beginning of the A1 trend (sensu Weibel et al., 2010): Thin opal rim - recrystallization of opal into cryptocrystalline quartz – continued growth of ordered microquartz (...).

Many elements of the diagenetic model (Weibel et al., 2010) were found in the grains studied; thus, it has been documented that opal and cryptocrystalline quartz rims, as well as opal lepispheres and microquartz, may be directly related to diagenesis. Another origin cannot be ruled out, especially in that the opal rims on the quartz grains may be related to chemical weathering of silicate minerals (e.g., Lee et al., 2007), which induces in situ formation of amorphous silica at silicate mineral surfaces and the release of silica into solution, followed by amorphous nanoparticle precipitation through inorganic processes (Williams and Crerar, 1985; Thiry et al., 2006; Liesegang and Milke, 2018). The presence of the opal may also be related, for example, to the concentration of the silicon-rich solution (Hallet, 1975) in the proglacial/subglacial zone of the ice sheet during alternating cycles of thawing and freezing in isolated water bodies under the ice cover (Blackburn et al., 2020). Rounded quartz overgrowths have been found from several stratigraphic intervals and geographic locations worldwide (Haile et al., 2021 and the references therein), including the Barents Sea Basin (e.g., the Upper Triassic to Middle Jurassic Wilhelmøya Subgroup on Svalbard; Haile et al., 2021). The presence of microcrystalline, cryptocrystalline and amorphous domains complicates the study of silica particles (Khouchaf et al., 2020).

As well as these issues related to various forms of silica, the nature and genesis of the Type B polymineralic coating requires further research. Consideration should start with cold environments, where polymineralic coatings can potentially form, because the loess in Poland represents the central part of the Northern European Loess Belt. This belt is considered to comprise classic ice-sheet loess (e.g., Gallet et al., 1998), presumably related to the Pleistocene glaciations (e.g., Jahn, 1950; Rousseau et al., 2014; Skurzyński et al., 2020), most likely blown from northern outwash plains (Smalley and Leach, 1978)
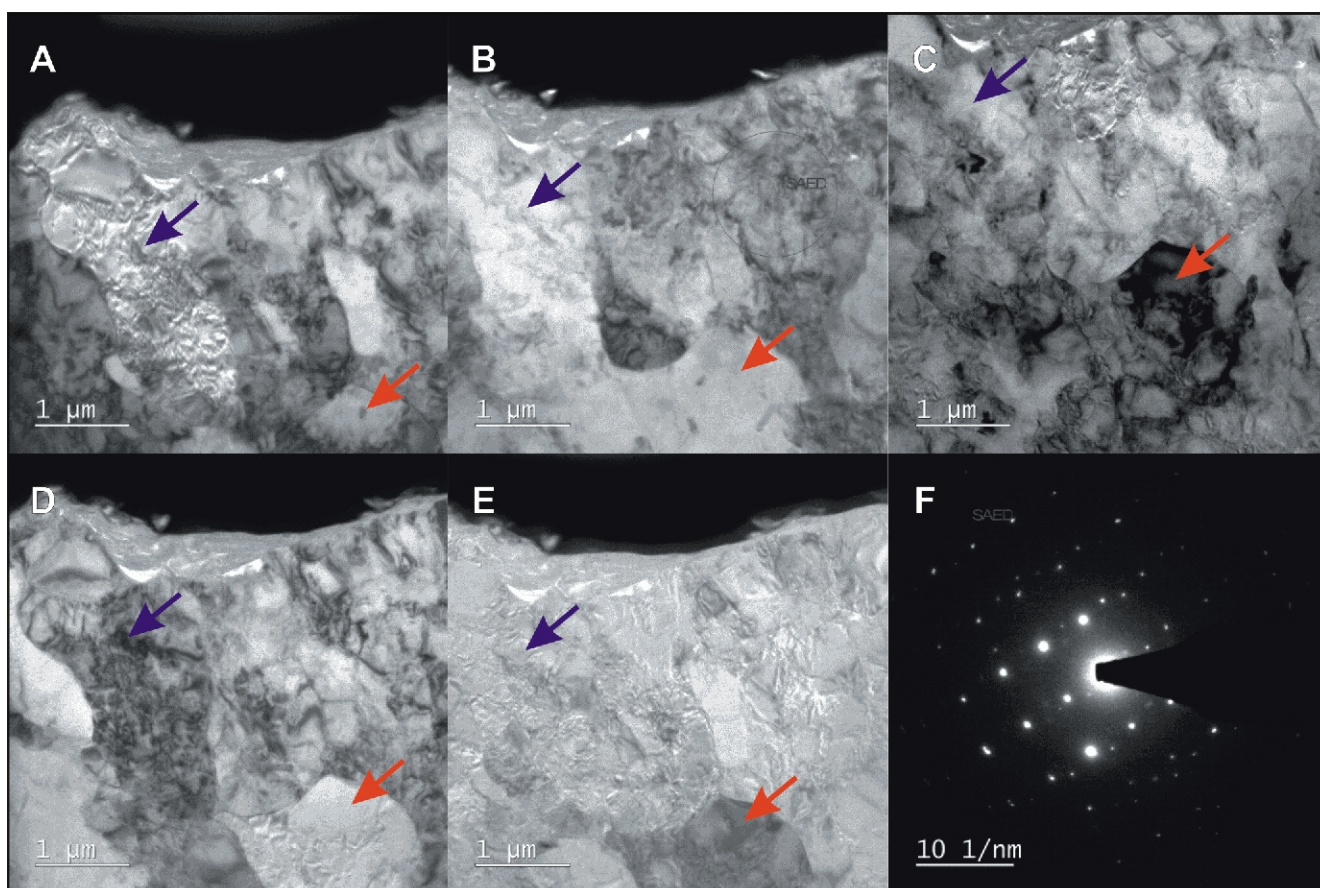
Fig. 8A–E – BF-TEM images of the same region of a lamella under different tilts of the sample, the coloured arrows are to indicate the same grain in all the images, varying bright and dark contrast in these images for a given grain is due to diffraction contrast; F – the selected area diffraction pattern from a quartz region also clearly indicating the polycrystalline nature of the quartz

or from sedimentary deposits previously redistributed by rivers (Badura et al., 2013; Baykal et al., 2021), with variable proportions of local geological material (Baykal et al., 2021). The presence of an initial coating was emphasized even for fresh glacial material collected directly from the glacier foreground (Stachnik et al., 2022), or for ice-core basal sediments (Blard et al., 2023). This is considered to be the product of Fe-sulphide weathering (e.g., pseudomorphs of Fe oxides after Fe-sulphides), aggregates cemented by Fe-oxides, and secondary Fe-oxide coatings around mineral grains (Stachnik et al., 2022). Coated grains formed at this early stage may easily be transported over long distances in various environments. Such coatings, rich in aluminum and iron oxides, may form both in low and high pH conditions, and once formed, are stable even at higher pH (Goldberg, 2008). As sediment distribution via rivers prior to short distance aeolian transport (Baykal et al., 2021) may have been of crucial importance for Polish loess deposition, the formation of a polymineralic coating in places located near to aqueous environments (e.g., Wooldridge et al., 2019), or those covered by re-deposited and weathered fluvial deposits, also cannot be excluded.

Following transport-related processes, pedogenesis may modify the deposited material, alternating loess and soils comprising the typical stratigraphy. Considering post-depositional processes, Type A polymineralic coatings (unlike Type B) may also be related to soil processes. The significance of infiltration and pedogenesis for potentially similar structures have been

previously highlighted (e.g., Biernacka and Issmer, 1996; Li et al., 2016; Ural, 2021). The influence of soil development on the behaviour of silica cannot be disregarded, although many similarities to the diagenetic scheme were found. However, those processes are most relevant for residual soils, directly related to the underlying parent rock, in which pedogenetically-related etching features may reflect the prevailing pedogenic regime (Wilson, 2020). For soils of a non-residual character, including those of alluvial, glacial and aeolian nature (such as loess), the possibility that quartz grains have been through several weathering cycles (resulting in mixtures of fresh and highly weathered grains) is very high. Therefore their interpretation is problematic and calls for caution (Wilson, 2020).

The information provided above shows that aeolian-deposited quartz grains may have different types of coatings or rims, formed at different times and in different environmental conditions. In addition, quartz itself is one of the most common minerals in the Earth's crust and occurs ubiquitously in magmatic, metamorphic and sedimentary rocks. It is an important pathfinder mineral for the reconstruction of geological processes and palaeoclimatic conditions (Götze, 2018; Götze et al., 2021). The proposed TEM investigation of individual quartz grains from Polish loess may contribute significantly to the understanding of petrogenetic processes.

In addition to purely environmental considerations, the impact of such results on research methods based on detrital quartz, such as OSL, should be considered. The penetration
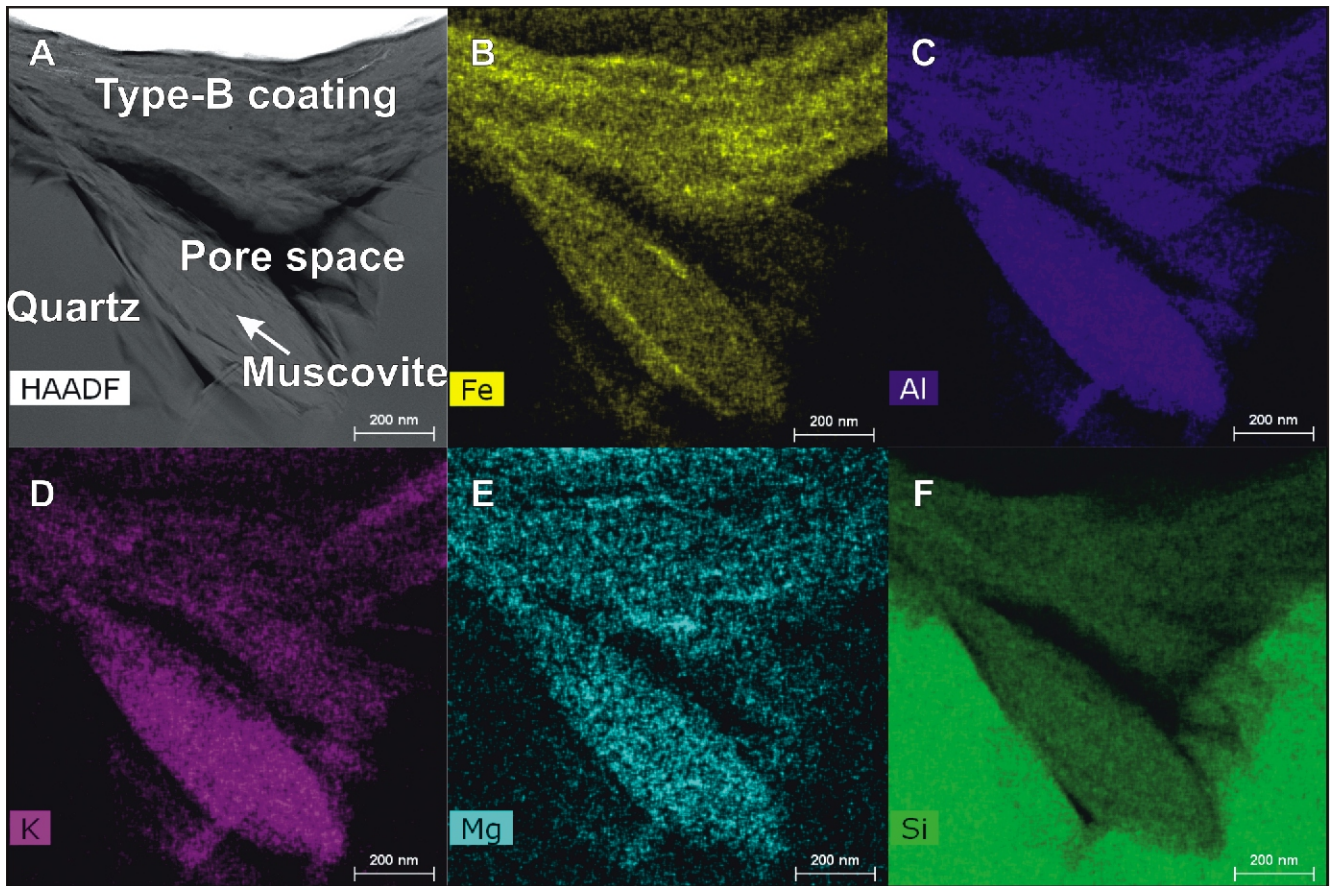
Fig. 9. HAADF-STEM image and corresponding EDS elemental maps showing the porous nature of the coating with a layered structure, the layers within the coating are mainly composed of Fe and Al and they are oriented parallel to the quartz surface below
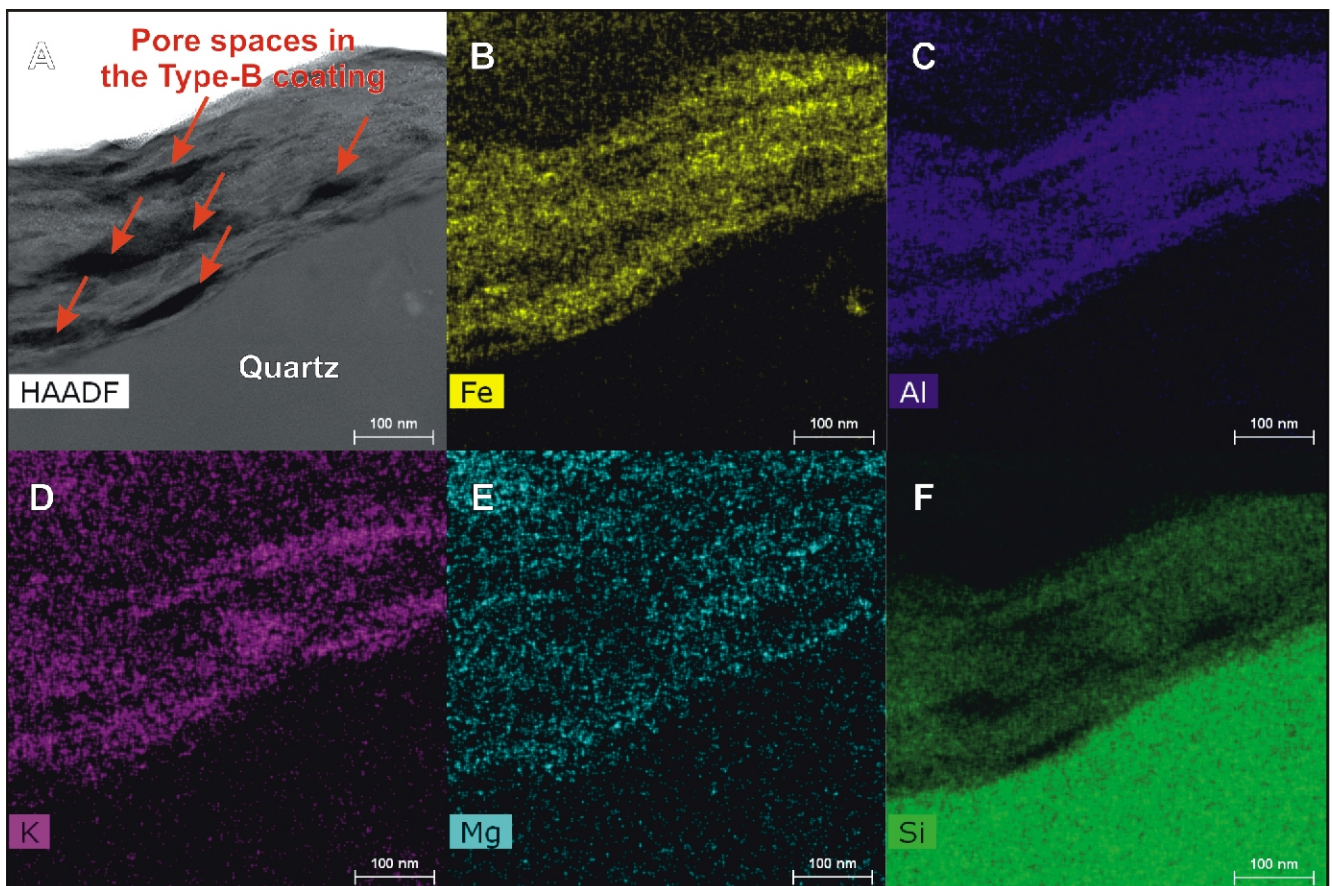

Fig. 10. The EDS maps and STEM image reveal layering of the coating, which is highlighted by Fe-enriched minerals (B) and aluminosilicates (C, F), the linear arrangement of these minerals is emphasized by the directional porosity seen in the STEM image (A), minerals rich in K and Mg also show a slight linear orientation (D, E)
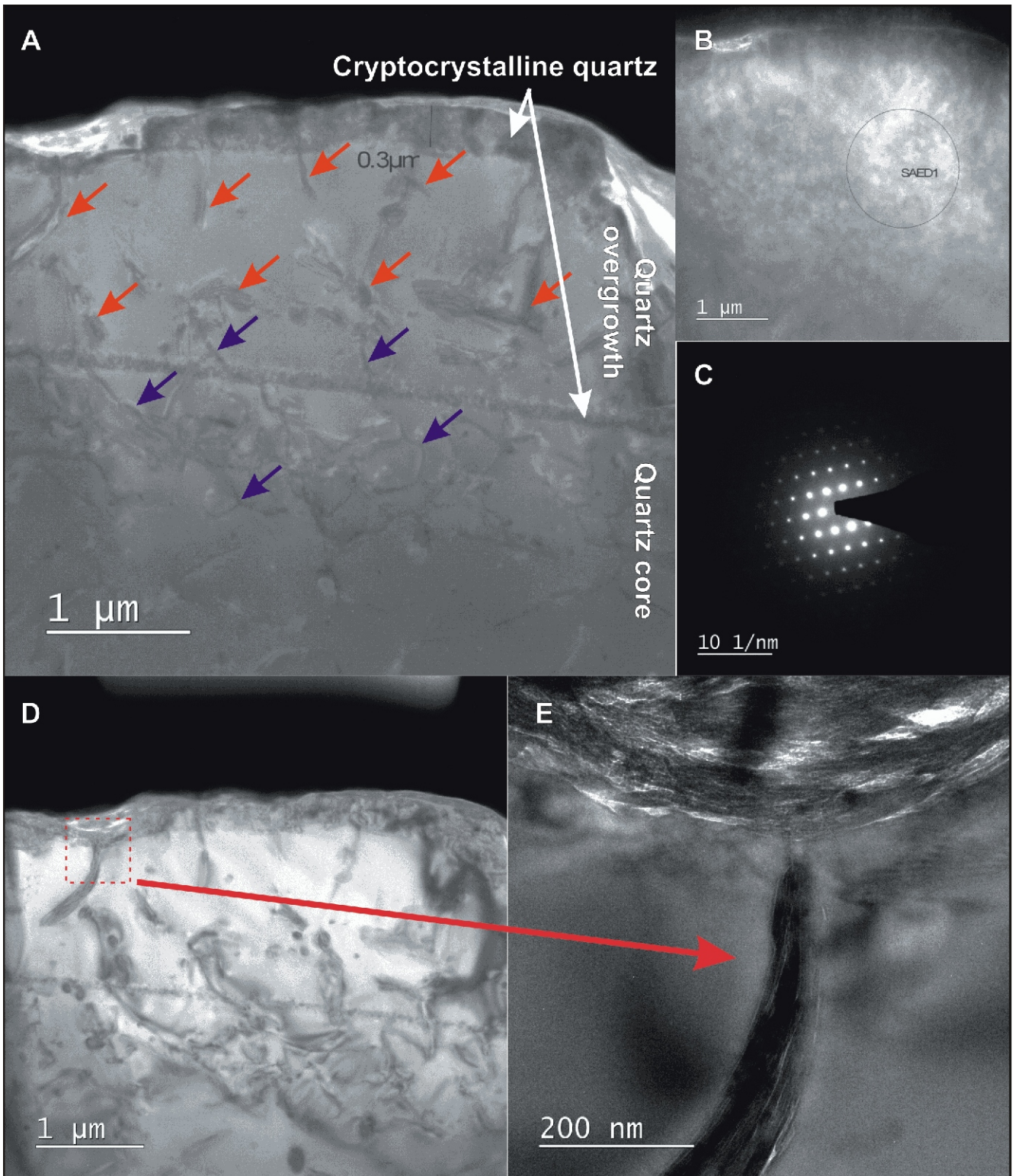
Fig. 11. TEM image of a cross-section showing the thin coating layer at the top (bright contrast) with varying thickness and cryptocrystalline quartz (A). This clearly indicates that the coating layers are on the surface of a larger particle of which the centre is constructed of three quartz generations – (1) quartz+mica core, (2) cryptocrystalline quartz, (3) quartz+mica overgrowth. Mica inclusions (red arrows) occur mainly above the inner cryptocrystalline rim. Structural defects occur both in the quartz interior and in a quartz outgrowth (blue arrows). The lack of an amorphous phase is confirmed by selected area electron diffraction shown in (C) from the marked quartz layer region in (B); this clearly shows that the quartz interior has a crystalline atomic structure
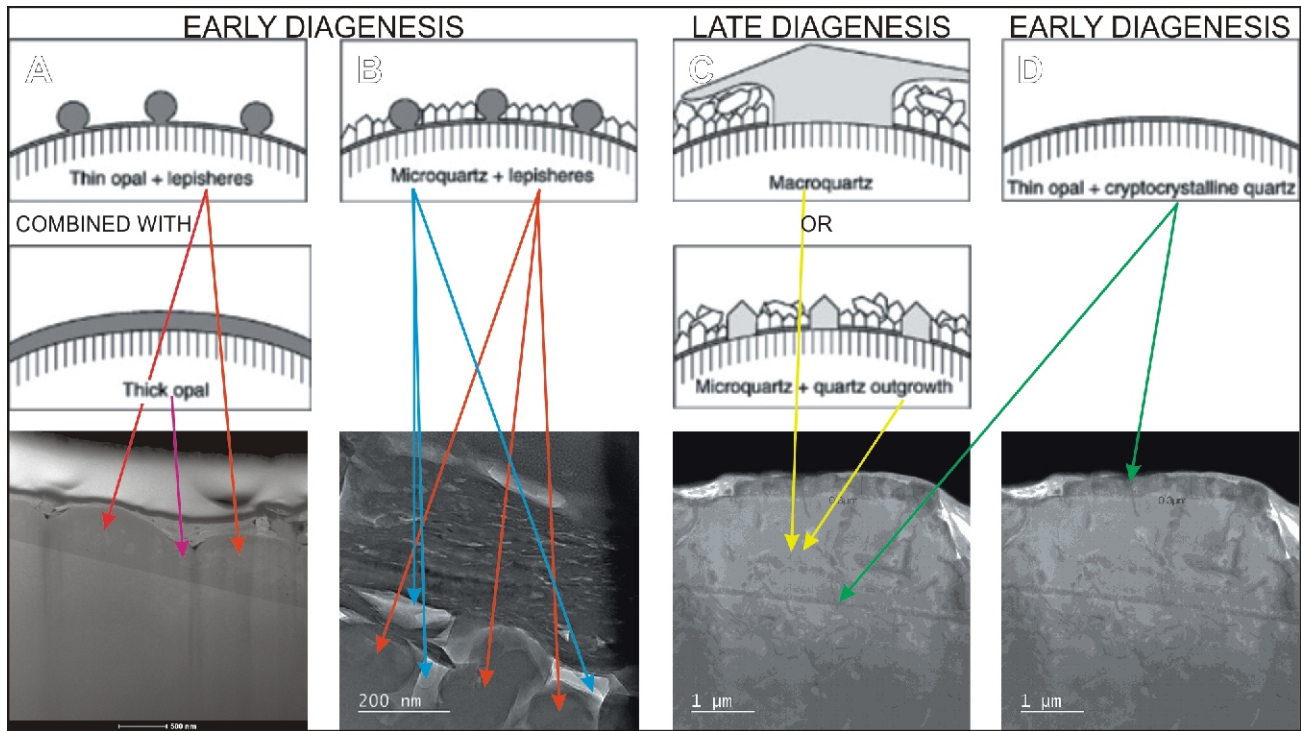
Fig. 12. External parts of grains analysed from Złota (A and B) and Tyszowce (C and D) against the background of elements of the schematic model of quartz authigenesis through early and late diagenesis (Weibel et al., 2010)

range-energy relation is known for quartz (particles with an energy of 1 MeV will have 3.3 µm of projected range in quartz; Berger et al., 1999) as well as for feldspar (which is not discussed here). This type of research was not conducted on opal (e.g., forming rims or lepispheres on diagenetically modified grains; Fig. 12) and in limited scale (Antohi-Trandafir et al., 2018) on muscovite (forming inclusions in quartz of the silt fraction; Fig. 11), therefore, the impact of such features on OSL dating remains unknown. An additional difficulty may be the mosaic crystal structure of quartz, clearly visible even in silt grains. This is certainly not a homogeneous quartz structure, but rather a polycrystalline form (Fig. 8). All of the above features result in the fact that the microphysical data obtained from a 'single' quartz grain may be the result of the interaction of numerous mineral grains, composed of different minerals (Jeong and Nousiainen, 2014).

All these characteristics of the quartz, and its opal/cryptocrystalline rims, most likely can influence the rate of HF etching. This is therefore not uniform and isotropic, and may directly influence the accuracy and precision of the estimated age as measured by OSL methods (e.g., Poręba et al., 2022). It can be also assumed that the internal structure, especially primary and secondary defects in quartz polycrystals, controls the susceptibility to HF acid etching (the acid, instead of digesting the particle on the surface, can potentially penetrate along cracks), similarly to the susceptibility to frost-induced modifications (especially cracks or even fragmentation) found for quartz sand grains (Górska et al., 2023). In addition, if the strongly adhesive Type B polymineralic coating is not completely removed (the quality of coating removal is never confirmed – it is assumed that quartz grains are single crystals; Bell and Zimmer-

man, 1978; Moska et al., 2021) in the initial phase of the preparation (by HCl and perhydrol), as a result of the reaction of HF with elements such as Mo, Fe and Cr, the surface of the etched grain may be covered by a passive film which hinders further corrosion (Dai et al., 2021).

Factors such as microporosity, mineralogical composition, coating structure and grain morphology resulting from these features may have a substantial impact on the interpretation of dust and soil properties such as dust generation, grain size distribution, deflation potential, sedimentation, diffusion, and optical scattering and absorption (Harrison et al., 2001). For example, the highly porous nature of the opal or crypto/microcrystalline rims, and the polymineralic coating, can determine the size/range dependence between particles and transport distance. This is the basis of the giant loess particle hypothesis (e.g., Jeong et al., 2014). The porous nature of the rims or coatings may also lead to incorrect results concerning density separation of the material, e.g. used for further OSL tests (e.g., Moska et al., 2021).

Due to these issues the quartz may be of key direct (e.g. interpretation of environmental history of the elements of the coating) or indirect (e.g., for OSL dating) importance for the restoration of palaeoenvironmental processes. Investigations of this nature will also benefit research into dust optical properties (Kandler et al., 2007; Moosmüller et al., 2012; Jeong and Nousiainen, 2014; Engelbrecht et al., 2016), remote sensing and dust transport modeling (Falkovich et al., 2001; Sima et al., 2009, 2013; Tian et al., 2015; Rousseau and Hatté, 2021; Torre et al., 2022), and the collapsibility of loess (Shao et al., 2018; Wang et al., 2021; Yang et al., 2022).

CONCLUSIONS

Preliminary analysis of aeolian quartz grains (representing loess sections from different regions of Poland), based on SEM imaging of ion-thinned bulk sample cross-sections, showed that part of the polymineralic surface coating is heterogeneous, and can can be divided into: (1) a relatively coarse (up to ten or so microns) part of openwork character, made mainly of randomly arranged minerals of lamellar shape (Type A), and (2) a finer part, adhering relatively closely to the grain, usually filling cavities and gaps on the grain surface (Type B).

Detailed S/TEM investigation reveals that the highly porous Type B polymineralic coating (composed of Fe oxides/hydroxides, Al-silicates, and some relatively coarse incorporated crystals such as anhedral potassium feldspar and idiomorphic hematite) may be disordered or arranged in a laminar pattern, and lie directly on the quartz surface or be separated from it by a thin layer of opal (with lepispheres) or cryptocrystalline quartz, most likely of diagenetic origin.

Apart from various types of coatings and rims, the aeolian quartz grain may have a complicated internal structure. The grains investigated, despite their small size, are characterized by a polycrystalline monomineral, or even be polycrystalline with a polymineralic composition (with numerous inclusions of muscovite) and internal structure.

These factors may strongly affect the perception of palaeoenvironmental proxy data, for example the highly porous nature of the polymineralic coating may result in a greater range of dust particle transport; and the complicated internal structure of the coated quartz grain may cause inaccuracies in age estimation using the OSL method. These issues require further research, and the methodology presented by us is a step towards such further investigations.

The refined methodology for investigation of coatings and near-surface regions of individual aeolian quartz grains, including SEM/FIB cross-section lamella preparation and further S/TEM characterization, preceded by investigation of ion-thinned cross-sections of bulk samples, offers interpretative possibilities which may be found useful by other groups working in palaeoenvironmental and related research.

REFERENCES

Aitken, M.J., 1985. Thermoluminescence Dating. Academic Press, London.

Aitken, M.J., 1998. An Introduction to Optical Dating. Oxford University Press, Oxford.

Antohi-Trandafir, O., Timar-Gabor, A., Vulpoi, A., Bălc, R., Longman, J., Veres, D., Simon, S., 2018. Luminescence properties of natural muscovite relevant to optical dating of contaminated quartz samples. Radiation Measurements, 109: 1–7; https://doi.org/10.1016/j.radmeas.2017.12.004

Arnold, H., 1962. Die Struktur des Hochquarzes. Zeitschrift für Kristallographie, 117: 467–469; https://doi.org/10.1524/zkri.1962.117.16.467

Badura, J., Jary, Z., Smalley, I., 2013. Sources of loess material for deposits in Poland and parts of Central Europe: the lost big river. Quaternary International, 296: 15–22; https://doi.org/10.1016/j.quaint.2012.06.019

Baykal, Y., Stevens, T., Engstrom-Johansson, A., Skurzyński, J., Zhang, H., He, J., Lu, H., Adamiec, G., Kotlinger, C., Jary, Z., 2021. Detrital zircon UePb U-Pb age analysis of last glacial loess sources and proglacial sediment dynamics in the Northern European Plain. Quaternary Science Reviews, 274: 107265; https://doi.org/10.1016/j.quascirev.2021.107265

Bell, W.T., Zimmerman, D.W., 1978. The effect of Hf acid etching on the morphology of quartz inclusions for thermoluminescence dating. Archaeometry, 20: 63–65; https://doi.org/10.1111/j.1475-4754.1978.tb00213.x

Berger, M., Coursey, J., Zucker, M., 1999. ESTAR, PSTAR, and ASTAR: Computer programs for calculating stopping-power and range tables for electrons, protons, and Helium Ions (version 1.21); http://physics.nist.gov/Star

Biernacka, J., Issmer, K., 1996. Micromorphological analysis of loess deposits from Klępicz, Western Pomerania (in Polish with English summary). Przegląd Geologiczny, 44: 43–48.

Blackburn, T., Edwards, G.H., Tulaczyk, S., Scudder, M., Piccione, G., Hallet, B., McLean, N., Zachos, J.C., Cheney, B., Babbe, J.T., 2020. Ice retreat in Wilkes Basin of East Antarctica during a warm interglacial. Nature, 583: 554–559; https://doi.org/10.1038/s41586-020-2484-5

Blanco, A., Zavala, F.J., Hernández-Ávila, J., Maurrasse, F., Duque-Botero, F., Ramírez-Cardona, M., 2010. Microbial preservation in sedimentary pyrite from Cretaceous organic-matter-rich carbonate mudstone: a preliminary report. 41st Annual Lunar and Planetary Science Conference, 1533: 2487.

Blard, P.-H., Protin, M., Tison, J-L., Fripiat, F., Dahl-Jensen, D., Steffensen, J.P., Mahaney, W.C., Bierman, P.R., Christ, A.J., Corbett, L.B., Debaille, V., Rigaudier, T., Claeys, P., ASTER Team., 2023. Basal debris of the NEEM ice core, Greenland: a window into sub-ice-sheet geology, basal ice processes and ice-sheet oscillations. Journal of Glaciology: 1–19; https://doi.org/10.1017/jog.2022.122

Dai, H., Shi, S., Yang, L., Guo, C., Chen, X., 2021. Recent progress on the corrosion behaviour of metallic materials in HF solution. Corrosion Reviews, 39: 313–337; https://doi.org/10.1515/corrrev-2020-0101

Downs, R.T., Bartelmehs, K.L., Gibbs, G.V., Boisen, M.B., 1993. Interactive software for calculating and displaying X-ray or neutron powder diffractometer patterns of crystalline materials. American Mineralogist, 78: 1104–1107.

Duval, M., Guilarte, V., Campana, I., Arnold, L.J., Miguens, L., Iglesias, J., Gonzalez-Sierra, S., 2018. Quantifying hydrofluoric acid etching of quartz and feldspar coarse grains based on weight loss estimates: Implication for ESR and luminescence dating studies. Ancient TL, 36: 1–14.

Engelbrecht, J.P., Moosmüller, H., Pincock, S., Jayanty, R.K.M., Lersch, T., Casuccio, G., 2016. Mineralogical, chemical, morphological, and optical interrelationships of mineral dust re-suspensions. Atmospheric Chemistry and Physics, 16: 10809–10830; https://doi.org/10.5194/acp-16-10809-2016, 2016

Falkovich, A.H., Ganor, E., Levin, Z., Formenti, P., Rudich, Y., 2001. Chemical and mineralogical analysis of individual mineral dust particles. Journal of Geophysical Research - Atmospheres, 106: 18029–18036; https://doi.org/10.1029/2000JD900430

Flörke, O.W., Hollmann, R., von Rad, U., Rösch, H., 1976. Intergrowth and twinning in opal-CT lepispheres. Contributions to Mineralogy and Petrology, 58: 235–242; https://doi.org/10.1007/BF00402354

Frederickson, A.F., 1955. Mosaic structure in quartz. Journal of the Mineralogical Society of America, 40: 1–9.

Gallet, S., Jahn, B., Van Vliet Lanoe, B., Dia, A., Rossello, E., 1998. Loess geochemistry and its implications for particle origin and composition of the upper continental crust. Earth and Planetary Science Letters, 156: 157–172; https://doi.org/10.1016/S0012-821X(97)00218-5

Goldberg, S., 2008. Interaction of aluminum and iron oxides and clay minerals and their effect on soil physical properties: A review. Communications in Soil Science and Plant Analysis, 20: 11–12; https://doi.org/10.1080/00103629009368144

Górska, M.E., Woronko, B., Kossowski, T.M., 2023. Factors influencing the development of microtextures on cold-climate aeolian quartz grains revealed by experimental frost action. Permafrost and Periglacial Processes; https://doi.org/10.1002/ppp.2179

Götze, J., 2018. Chemistry, textures and physical properties of quartz – geological interpretation and technical application. Mineralogical Magazine, 73: 645–671; https://doi.org/10.1180/minmag.2009.073.4.645

Götze, J., Pan, Y., Müller, A., 2021. Mineralogy and mineral chemistry of quartz: a review. Mineralogical Magazine, 85: 639–664; https://doi.org/10.1180/mgm.2021.72

Grabowska-Olszewska, B., 1983. Osiadanie zapadowe lessów w świetle badań mikrostrukturalnych (in Polish with English summary). Przegląd Geologiczny, 31: 162–165.

Haile, B.G., Line, L.H., Klausen, T.G., Olaussen, S., Eide, C.H., Jahren, J., Hellevang, H., 2021. Quartz overgrowth textures and fluid inclusion thermometry evidence for basin-scale sedimentary recycling: An example from the Mesozoic Barents Sea Basin. Basin Research, 33: 1697–1710; https://doi.org/10.1111/bre.12531

Hallet, B., 1975. Subglacial silica deposits. Nature, 254: 682–683; https://doi.org/10.1038/254682a0

Harrison, S.P., Kohfeld, K.E., Roelandt, C., Claquin, T., 2001. The role of dust in climate changes today, at the last glacial maximum and in the future. Earth-Science Reviews, 54: 43–80; https://doi.org/10.1016/S0012-8252(01)00041-1

Hirose, T., Kihara, K., Okuno, M., Fujinami, S., Shinoda, K., 2005. X-ray, DTA and Raman studies of monoclinic tridymite and its higher temperature orthorhombic modification with varying temperature. Journal of Mineralogical and Petrological Sciences, 100: 55–69; https://ui.adsabs.harvard.edu/link_gateway/2005JMPeS.100...55H/doi:10.2465/jmps.100.55

Hrstka, T., Gottlieb, P., Skala, R., Breiter, K., Motl, D., 2018. Automated mineralogy and petrology-applications of TESCAN Integrated Mineral Analyzer (TIMA). Journal of Geosciences, 63: 47–63; http://doi.org/10.3190/jgeosci.250

Ikuta, D., Kawame, N., Banno, S., Hirajima, T., Ito, K., Rakovan, J.F., Downs, R.T., Tamada, O., 2007. First in situ X-ray identification of coesite and retrograde quartz on a glass thin section of an ultrahigh-pressure metamorphic rock and their crystal structure details. American Mineralogist, 92: 57–63; https://doi.org/10.2138/am.2007.2228

Jahn, A., 1950. Loess, its origin and connection with the climate of the glacial epoch (in Polish with English summary). Acta Geologica Polonica, 1: 257–310.

Jeong, G.Y., 2008. Bulk and single-particle mineralogy of Asian dust and a comparison with its source soils. Journal of geophysical research. Atmospheres, 113: D02208; https://doi.org/10.1029/2007JD008606

Jeong, G.Y., Nousiainen, T., 2014. TEM analysis of the internal structures and mineralogy of Asian dust particles and the implications for optical modelling. Atmospheric Chemistry and Physics, 14: 7233–7254; https://doi.org/10.5194/acp-14-7233-2014

Jeong, G.Y., Kim, J.Y., Seo, J., Kim, G.M., Jin, H.C., Chun, Y., 2014. Long-range transport of giant particles in Asian dust identified by physical, mineralogical, and meteorological analysis. Atmospheric Chemistry and Physics, 14: 505–521; https://doi.org/10.5194/acp-14-505-2014

Kandler, K., Benker, N., Bundke, U., Cuevas, E., Ebert, M., Knippertz, P., Rodriguez, S., Schutz, L., Weinbruch, S., 2007. Chemical composition and complex refractive index of Saharan Mineral Dust at Izaña, Tenerife (Spain) derived by electron microscopy. Atmospheric Environment, 41: 8058–8074; https://doi.org/10.1016/j.atmosenv.2007.06.047

Kenis, P., Skurzyński, J., Jary, Z., Kubik, R., 2020. A new methodological approach (QEMSCAN®) in the mineralogical study of Polish loess: Guidelines for further research. Open Geosciences, 12: 342–353; https://doi.org/10.1515/geo-2020-0138

Khouchaf, L., Boulahya, K., Pratim, Das, P., Nicolopoulos, S., Kovacs Kis, V., Labar, J.L., 2020. Study of the Microstructure of Amorphous Silica Nanostructures Using High-Resolution Electron Microscopy, Electron Energy Loss Spectroscopy, X-ray Powder Diffraction, and Electron Pair Distribution Function. Materials, 13: 4393; https://doi.org/10.3390/ma13194393

Lee, M.K., Natter, M., Keevan, J., Guerra, K., Saunders, J., Uddin, A., Humayun, M., Wang, Y., Keimowitz, A.R., 2013. Assessing effects of climate change on biogeochemical cycling of trace metals in alluvial and coastal watersheds. British Journal of Environment and Climate Change, 3: 44–66; https://doi.org/10.9734/BJECC/2013/3061

Lee, M.R., Brown, D.J., Smith, C.L., Hodson, M.E., MacKenzie, M., Hellmann, R., 2007. Characterization of mineral surfaces using FIB and TEM: A case study of naturally weathered alkali feldspars. American Mineralogists, 92: 1383–1394; https://doi.org/10.2138/am.2007.2453

Lehmkuhl, F., Nett, J.J., Potter, S., Schulte, P., Sprafke, T., Jary, Z., Antoine, P., Wacha, L., Wolf, D., Zerboni, A., Hosek, J., Marković, S.B., Obreht, I., Sumegi, P., Veres, D., Zeeden, C., Boemke, B., Schaubert, V., Viehweger, J., Hambach, U., 2021. Loess landscapes of Europe – mapping, geomorphology, and zonal differentiation. Earth-Science Reviews, 215: 103496; https://doi.org/10.1016/j.earscirev.2020.103496

Levien, L., Prewitt, C.T., Weidner, D.J., 1980. Structure and elastic properties of quartz at pressure. American Mineralogist, 65: 920–930.

Li, Z., Xu, R., Li, J., Hong, Z., 2016. Effect of clay colloids on the zeta potential of Fe/Al oxide-coated quartz: a streaming potential study. Journal of Soils and Sediments, 16: 2676–2686; https://doi.org/10.1007/s11368-016-1463-9

Liesegang, M., Milke, R., 2018. Silica colloid ordering in a dynamic sedimentary environment. Minerals, 8: 12; https://doi.org/10.3390/min8010012

Marković, S.B, Bokhorst, M., Vanderberghe, J., McCoy ,W., Oches, E., Hambach, U., 2008. Late Pleistocene loess-paleosol sequences in the Vojvodina region, north Serbia. Journal of Quaternary Science, 23: 73–84; http://dx.doi.org/10.1002/jqs.1124

Marković, S.B, Stevens, T., Kukla, G.J., Hambach, U., Fitzsimmons, K.E., Gibbard, P., Buggle, B., Zech, M., Guo, Z., Hao, Q., Wu, H., Ken, O'Hara D., Smalley, J., Ujvari, G., Sümegi, P., Timar-Gabor, A., Veres, D., Sirocko, F., Vasilijević, A., Jary, Z., Svensson, A., Jović, V., Lehmkuhl, F., Kovacs, J., Svircev, Z. 2015. Danube loess stratigraphy – Towards a pan-European loess stratigraphic model. Quaternary Science Reviews, 148: 228–258; https://doi.org/10.1016/j.earscirev.2015.06.005

Maruszczak, H., 1991. General features of the loesses in Poland (in Polish with English summary). In: Podstawowe profile lessów w Polsce (Main section of loesses in Poland) (ed. H. Maruszczak). Wyd. UMCS, Lublin.

Moosmüller, H., Engelbrecht, J.P., Skiba, M., Frey, G., Chakrabarty, R.K., Arnott, P., 2012. Single scattering albedo of fine mineral dust aerosols controlled by iron concentration. Journal of Geophysical Research, 117: D11210; https://doi.org/10.1029/2011JD016909

Moska, P., 2019. Luminescence dating of Quaternary sediments – some practical aspects. Studia Quaternaria, 36: 2161–169; https://doi.org/10.24425/sq.2019.126387

Moska, P., Adamiec, G., Jary, Z., Bluszcz, A., 2017. OSL chronostratigraphy for loess deposits from Tyszowce – Poland. Geochronometria, 44: 307–318; https://doi.org/10.1515/geochr-2015-0074

Moska, P., Adamiec, G., Jary, Z., Bluszcz, A., Poręba, G., Piotrowska, N., Krawczyk, M., Skurzyński, J., 2018. Luminescence chronostratigraphy for the loess deposits in Złota, Poland. Geochronometria, 45: 44–55; http://dx.doi.org/10.1515/geochr-2015-0073

Moska, P., Jary, Z., Adamiec, G., Bluszcz, A., 2019. Chronostratigraphy of a loess-palaeosol sequence in Biały Kościół, Poland using OSL and radiocarbon dating. Quaternary International, 502: 4–17; https://doi.org/10.1016/j.quaint.2018.05.024

Moska, P., Bluszcz, A., Poręba, G., Tudyka, K., Adamiec, G., Szymak, A., Przybyła, A., 2021. Luminescence dating procedures at the Gliwice luminescence dating laboratory. Geochronometria, 48: 1–15; https://doi.org/10.2478/geochr-2021-0001

Porat, N., Faerstein, G., Medialdea, A., Murray, A.S., 2015. Re-examination of common extraction and purification methods of quartz and feldspar for luminescence dating. Ancient TL, 33: 9.

Poręba, G., Tudyka, K., Szymak, A., Pluta, J., Rocznik, J., Świątkowski, J., Osadnik, R., Moska, P., 2022. Evaluating the effect of hydrofluoric acid etching on quartz grains using microscope image analysis, laser diffraction and weight loss particle size estimate. Geochronometria, 49: 1–8; https://doi.org/10.2478/geochr-2022-0001

Rousseau, D.-D., Hatté, C., 2021. Ground-Air Interface: The Loess Sequences, Markers of Atmospheric Circulation. In: Paleoclimatology (eds. G. Ramstein, A. Landais, N. Bouttes, P. Sepulchre, A. Govin) Frontiers in Earth Sciences. Springer, Cham; https://doi.org/10.1007/978-3-030-24982-3_13

Rousseau, D.-D., Chauvel, C., Sima, A., Hatte, C., Lagroix, F., Antoine, P., Balkanski, Y., Fuchs, M., Mellett, C., Kageyama, M., Ramstein, G., Lang, A., 2014. European glacial dust deposits: Geochemical constraints on atmospheric dust cycle modeling. Geophysical Research Letters, 41: 7666–7674; https://doi.org/10.1002/2014GL061382

Schaffer, M., Schaffer, B., Ramasse, Q., 2012. Sample preparation for atomic-resolution STEM at low voltages by FIB. Ultramicroscopy, 114: 62–71; https://doi.org/10.1016/j.ultramic.2012.01.005

Shao, X., Zhang, H., Tan, Y., 2018. Collapse behavior and microstructural alteration of remolded loess under graded wetting tests. Engineering Geology, 233: 11–22; https://doi.org/10.1016/j.enggeo.2017.11.025

Sima, A., Rousseau, D.-D., Kageyama, M., Ramstein, G., Schultz, M., Balkanski, Y., Antoine, P., Dulac, F., Hatté, C., 2009. Imprint of North-Atlantic abrupt climate changes on western European loess deposits as viewed in a dust emission model. Quaternary Science Reviews, 28: 2851–2866; https://doi.org/10.1016/j.quascirev.2009.07.016

Sima, A., Kageyama, M., Rousseau, D.-D., Ramstein, G., Balkanski, Y., Antoine, P., Hatté, C., 2013. Modeling dust emission response to North Atlantic millennial-scale climate variations from the perspective of East European MIS 3 loess deposits. Climate of the Past, 9: 1385–1402; https://doi.org/10.5194/cp-9-1385-2013, 2013

Skurzyński, J., Jary, Z., Raczyk, J., Moska, P., Korabiewski, B., Ryzner, K., Krawczyk, M., 2019. Geochemical characterization of the Late Pleistocene loess-palaeosol sequence in Tyszowce (Sokal Plateau-Ridge, SE Poland). Quaternary International, 502: 108–118; https://doi.org/10.1016/j.quaint.2018.04.023

Skurzyński, J., Jary, Z., Kenis, P., Kubik, R., Moska, P., Raczyk, J., Seul, C., 2020. Geochemistry and mineralogy of the Late Pleistocene loess-palaeosol sequence in Złota (near Sandomierz, Poland): implications for weathering, sedimentary recycling and provenance. Geoderma, 375: 114459; https://doi.org/10.1016/j.geoderma.2020.114459

Smalley, I.J., Leach, J.A., 1978. The origin and distribution of the loess in the Danube basin and associated regions of East-Central Europe: a review. Sedimentary Geology, 21: 1–26; https://doi.org/10.1016/0037-0738(78)90031-3

Smalley, I.J., Vita-Finzi, C., 1968. The formation of fine particles in sandy deserts and the nature of "desert" loess. Journal of Sedimentary Petrology, 38: 766–774; https://doi.org/10.1306/74D71A69-2B21-11D7-8648000102C1865D

Stachnik, Ł., Yde, J.C., Krzemień, K., Uzarowicz, Ł., Sitek, S., Kenis, P., 2022. SEM-EDS and water chemistry characteristics at the early stages of glacier recession reveal biogeochemical coupling between proglacial sediments and meltwater. Science of The Total Environment, 835: 155383; https://doi.org/10.1016/j.scitotenv.2022.155383

Thiry, M., Milnes, A.R., Rayot, V., Simon-Coinçon, S., 2006. Interpretation of palaeoweathering features and successive silicifications in the Tertiary regolith of Inland Australia. Journal of Geological Society, 163: 723–736; http://dx.doi.org/10.1144/0014-764905-020

Tian, P., Cao, X., Zhang, L., Wang, H., Shi, J., Huang, Z., Zhou, T., Liu, H., 2015. Observation and simulation study of atmospheric aerosol nonsphericity over the Loess Plateau in northwest China. Atmospheric Environment, 117: 212–219; https://doi.org/10.1016/j.atmosenv.2015.07.020

Torre, G., Gaiero, D., Coppo, R., Cosentino, N.J., Goldstein, S.L., De Vleeschouwer, F., Le Roux, G., Bolge, L., Kiro, Y., Sawakuchi, A.O., 2022. Unraveling late Quaternary atmospheric circulation in the Southern Hemisphere through the provenance of Pampean loess. Earth-Science Reviews, 232: 104143; https://doi.org/10.1016/j.earscirev.2022.104143

Ural, N., 2021. The significance of scanning electron microscopy (SEM) analysis on the microstructure of improved clay: An overview. Open Geosciences, 13: 197–218; https://doi.org/10.1515/geo-2020-0145

Wang, H., Ni, W., Yuan, K., Nie, Y., Guo, Y., 2021. Microstructure evolution of loess under multiple collapsibility based on nuclear magnetic resonance and scanning electron microscopy. Journal of Mountain Science, 18: 2612–2625; https://doi.org/10.1007/s11629-021-6838-8

Weibel, R., Friis, H., Kazerouni, A. M., Svendsen, J. B., Stokkendal, J., Poulsen, M.L.K., 2010. Development of early diagenetic silica and quartz morphologies – examples from the Siri Canyon, Danish North Sea. Sedimentary Geology, 228: 151–170; https://doi.org/10.1016/j.sedgeo.2010.04.008

Williams, L.A., Crerar, D.A., 1985. Silica diagenesis, II, General mechanisms. Journal of Sedimentary Petrology, 55: 312–321; https://doi.org/10.1306/212F86B1-2B24-11D7-8648000102C1865D

Wilson, M.J., 2020. Dissolution and formation of quartz in soil environments: a review. Soil Science Annual, 71: 99–110; https://doi.org/10.37501/soilsa/122398

Wooldridge, L.J., Worden, R.H., Griffiths, J., Utley, J.E., 2019. How to quantify clay-coat grain coverage in modern and ancient sediments. Journal of Sedimentary Research, 89: 135–146; https://doi.org/10.2110/jsr.2019.6

Yang, H., Xie, W., Liu, Q., Zhu, R., Liu, Y., 2022. Three-stage collapsibility evolution of Malan loess in the Loess Plateau. Catena, 217: 106482; https://doi.org/10.1016/j.catena.2022.106482